Wide-range thin-film ceramic–metal-alloy thermometers with low magnetoresistance

N.A. Fortune,[1,*] J.E. Palmer-Fortune,[1,†] A. Trainer,[1] A. Bangura,[2] N. Kondedan,[3,‡] and A. Rydh[3]

[1] *Department of Physics, Smith College, Northampton, Massachusetts 01063, USA*
[2] *National High Magnetic Field Laboratory, Tallahassee, Florida 32310, USA*
[3] *Department of Physics, Stockholm University, AlbaNova University Center, Stockholm SE-106 91, Sweden*

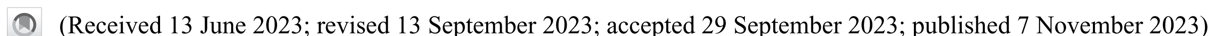

(Received 13 June 2023; revised 13 September 2023; accepted 29 September 2023; published 7 November 2023)

Many thermal measurements in high magnetic fields—including heat capacity, thermal conductivity, thermopower, magnetocaloric, and thermal-Hall-effect measurements—require thermometers that are sensitive over a wide temperature range, are low mass, have a rapid thermal response, and have a minimal easily correctable magnetoresistance. Here, we report the development of a granular-metal oxide ceramic composite (cermet) for this purpose formed by cosputtering of the metallic alloy nichrome ($Ni_{0.8}Cr_{0.2}$) and the insulator silicon dioxide (SiO_2). We find that cosputtering of Ni-Cr alloys with SiO_2 in a reactive-oxygen plus inert-argon-gas mixture produces resistive thin-film thermometers sensitive enough to be used in calorimetry and related measurements from room temperature down to below 100 mK in magnetic fields up to at least 41 T.

DOI: 10.1103/PhysRevApplied.20.054016

I. INTRODUCTION

Magnetic field dependent small-sample calorimetric and related thermal measurements [1,2] impose a particularly stringent set of requirements on the materials used for resistive thermometry. The thermometers should (1) have a resistance $R(T)$ that depends monotonically on temperature T, (2) have a high dimensionless sensitivity (logarithmic derivative) $S = -d \log R / d \log T = -(T/R) dR/dT$ over a wide range of temperature, to resolve small changes in temperature ΔT over the full range of measurement, (3) be small and thin, to minimize the heat capacity and maximize the speed of the thermal response, (4) be stable at high temperature, so as not to lose calibration through general handling and temperature cycling, and (5) have a negligible magnetoresistance, so that changes in temperature can be distinguished from changes in field. Like all low-temperature thermometers, they also have a negative temperature coefficient (NTC) $dR/dT < 0$ so as to remain sensitive at low temperature. The most commonly used NTC resistive thermometers reported in the literature—thick-film ruthenium oxide [3–5], thin-film metal oxynitrides [6,7] such as the commercially available Cernox™ ZrO_xN_y [8], and thin amorphous or polycrystalline films of Au_xGe_{1-x} [9–13]—all exhibit some of these qualities but none satisfy all of these requirements over the full range of temperatures (< 100 mK to 300 K) and dc magnetic fields (0–45 T) available at sites such as the National High Magnetic Field Laboratory (NHMFL) [14].

Thick-film ruthenium oxide sensors prepared by screen printing of conductive paste containing ruthenium oxide and bismuth ruthenate have a smaller magnetoresistance than most other alternatives below 4 K [3–5,15] and dimensionless sensitivities between 0.25 and 0.5 at 1 K [4] but are largely insensitive at temperatures above 20 K [3, 16]. They also have a larger mass, slower thermal response, higher heat capacity, and poorer thermal contact than competing thin-film sensors. Thin-film versions designed to overcome these disadvantages exhibit much lower dimensionless sensitivity ($\lesssim 0.1$), making them unsuitable for high-resolution calorimetry [17].

Thin-film metal oxynitride MO_xN_y resistors (where M = Hf, Nb, Ti, Ta, and/or Zr) offer higher dimensionless sensitivities (in the range 0.5–2) that are useful over a much wider temperature range than RuO_x sensors. These sensors are grown by reactive sputtering of an elemental metal in a controlled mixture of oxygen and nitrogen gas [7,8]. Unfortunately, they are also highly magnetoresistive below 4 K—approaching 100% in a field of 15 T at 0.1 K [15,18].

Annealed polycrystalline films of Au_xGe_{1-x} offer low mass, rapid thermal response, and a high and tunable dimensionless sensitivity ranging from 0.5 to 2 between 30

*nfortune@smith.edu
†jfortune@smith.edu
‡neha.kondedan@fysik.su.se

 © 2023 American Physical Society

mK and 300 K [11,12] after annealing at 150–160°C, making them an attractive choice for zero-field nanocalorimetry [1]. They can also be readily fabricated through flash evaporation or cosputtering. The temperature dependence and sensitivity are, however, strongly dependent upon the annealing conditions, as these affect the size and distribution of the Au islands formed at the polycrystalline Ge grain boundaries [12]. Films annealed at these temperatures are therefore subject to shifts in calibration [12]. Also, these films exhibit significant magnetoresistance at low temperatures, reaching 20% in a 20-T field at 0.1 K [15]. Annealing at much higher temperatures (450°C) in a reducing atmosphere has recently [13] been reported to yield a stable reproducible sensor with a logarithmic temperature dependence but the reduced sensitivity ($S < 0.1$) makes it impractical for high-resolution calorimetry.

Less commonly used resistive thermometers include the ceramic-metal composites (cermets) [19–21] reinvestigated here. Cermets are produced by the cosputtering of a metal and an insulator, which produces weakly connected metallic islands in an insulating ceramic sea at metal concentrations close to the percolation threshold. Conduction primarily occurs due to thermally assisted hopping of charge carriers from island to island and is therefore strongly temperature dependent at low temperatures [22]. The relatively low magnetoresistance reported for several cermets in magnetic fields above a few tesla [20,21,23,24] has led us to take a second look at them for thermometry and small-sample calorimetry. Cermets can be prepared from several elemental metals combined with insulators such as SiO_2 and Al_2O_3 [19, and references therein].

The temperature dependence of resistance for a cermet is controlled by the distribution of island sizes, interisland distances, and metallic percentage [22,25], providing an opportunity for fine tuning the sensitivity through cosputtering in a manner not available using standard deposition methods for thick-film RuO_x and thin-film oxynitride MO_xN_y resistors. Observations of a pronounced low-field negative magnetoresistance [23] and reduced sensitivity [20,21] at low temperature have, however, limited their use for calorimetry and related measurements in magnetic fields [26]. These drawbacks turn out to arise from the particular materials used. Here, we switch from elemental metals to low-magnetoresistance metallic alloys and show that cosputtering of such alloys with SiO_2 in a reactive-oxygen plus inert-gas mixture produces resistive thin-film thermometers with both a high sensitivity over an extended temperature range and a significantly reduced magnetoresistance at low temperatures.

II. METHODS

A. Thin-film fabrication

In a first set of depositions, thin-film cermets were produced by the cosputtering of nichrome ($Ni_{0.8}Cr_{0.2}$, abbreviated here as Ni-Cr) and SiO_2 targets onto an insulating 150-nm-thick silicon-nitride-coated silicon substrate at room temperature (1000-nm silicon-oxide-coated silicon substrates produce equivalent results). Prior to deposition, the chamber was pumped down to a base pressure of $< 2 \times 10^{-8}$ Torr. The films were cosputtered in a working gas of Ar at 3 mTorr and a flow rate of 25 sccm. Typical deposition rates were 0.8–1.8 nm/min for Ni-Cr and 0.5–0.6 nm/min for SiO_2. Completed thin films had a thickness of 50–60 nm. The final composition was labeled by the Ni-Cr deposition fraction.

In a second set of depositions, a dilute Ar-O_2 mixture was substituted for pure Ar as the working gas. Typical deposition rates were 1.8–2.5 nm/min for Ni-Cr and 0.5–0.8 nm/min for SiO_2, producing thin films on the order of 50–60 nm. A protective cap of 15-nm-thick SiO_2 was deposited on top of the cermet films to prevent any subsequent reaction with the atmosphere. The depositions were done at a deposition pressure of 3 mTorr and a flow rate of 25 sccm Ar, with O_2 flow rates varying from 0.10–0.18 sccm. Before deposition, the chamber was pretreated with a Ar-O_2 gas mixture (4:1 flow-rate ratio, 30 mTorr, 5 min at room temperature). This pretreatment occurred after the chamber reached its base pressure of $< 2 \times 10^{-8}$ Torr and just prior to moving the sample from the load lock into the deposition chamber.

We note that base pressures and control over pretreatment conditions for different sputtering systems have a significant influence on the quality of the deposited films and their resulting temperature dependence. The results are strongly detrimentally affected by the presence of residual gases and/or oxygen-gettering materials left on the chamber walls from prior depositions. We have found that an ultrahigh vacuum and careful pretreatment of the sputter chamber (as described above) are needed to obtain reproducible results.

B. TEM

Plan-view TEM samples were prepared using well-known methods [27,28]. Briefly, 3-mm-diameter disks were cut from cermet films deposited on SiO_2-coated 280-μm-thick silicon substrates. A hand-polishing tool was used to polish the backside of the disks to a thickness of about 100 μm and a dimple grinder was used to polish the center of the disk to a thickness of approximately 5 μm. The samples were then placed in an ion mill (3 keV argon, 0.1 mA, at approximately 10° glancing incidence) and thinned from the backside until a small hole formed in the center. Images were made in the electron-transparent regions adjacent to the hole using a JEOL JEM-400 transmission electron microscope operated at 100 kV. The particle size was estimated by drawing a line of known length across the photograph and dividing the length by the number of particles along the line. This was done 3

times on each photograph and the average was reported as the estimated particle size.

C. Resistance measurements

All resistance measurements were performed at a temperature-dependent power (about 10 fW at 0.1 K, 1 pW at 1 K, and 10 nW at 100 K) chosen to avoid systematic errors due to self-heating. Magnetoresistance measurements require a constant temperature while sweeping a magnetic field; this was done by integrating the studied thermometer into a membrane-based nanocalorimeter [1]. A constant temperature was then obtained through a local-temperature offset heater at constant total heater power, raising the calorimeter-thermometer temperature above that of the cryostat bath. Measurements up to 12 T were taken in a dilution refrigerator with a stable base temperature below 10 mK (a dilution unit in a compensated magnetic field). The weak thermal coupling between the studied thermometer on the calorimeter and the thermal bath provides a very stable temperature that is insensitive to magnetic fields. For temperatures above 50 mK, any magnetic field effects on the cryostat will not affect the temperature on the calorimeter. A stable temperature can thus be obtained by measuring and stabilizing the total power supplied to the calorimeter area and assuming that the calorimeter thermal link is magnetic field independent. Measurements at low calorimeter power with insignificant offset heating but with stabilized base temperature up to 4 K confirm this assumption. Measurements at higher fields were taken at NHMFL in the same way, using a ^{3}He system. Magnetic field sweeps below 1 K were performed at very slow ramp rates (below 0.2 mT/s).

III. RESULTS

A. Temperature dependence

The temperature-dependent resistivities $\rho(T)$ (at zero field) for the first set of depositions (in argon) are shown in Fig. 1. Importantly, there is a crossover in the slope of the low-temperature dimensionless sensitivity from positive to negative with increasing metal percentage, with a nearly constant dimensionless sensitivity of 0.1 at 66.5% Ni-Cr metal fraction. This indicates that our samples span the transition region between insulating and metallic behavior [29]. Both the resistivity and the sensitivity increase with decreasing temperature for insulating samples, with the 62.5% sample representing the lower limit for the metal concentration for this particular cosputtering method (due to the large difference in metal and insulator sputtering rates).

In Fig. 2, the results from the second set of depositions in an Ar-O_2 atmosphere are shown for a set of three films (A, B, and C) deposited at constant Ni-Cr and SiO_2 sputtering rates but with differing oxygen flow rates. Also shown is

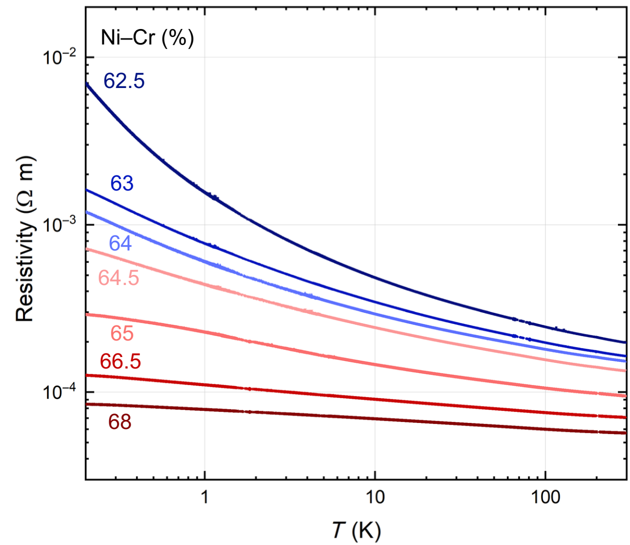

FIG. 1. The temperature-dependent resistivity as a function of the Ni-Cr percentage by volume for (Ni-Cr, SiO_2) cermets cosputtered in argon at 3 mTorr.

a film D deposited at a lower metal sputtering rate using an oxygen flow rate of 0.10 sccm. Sample C is metallic, while the other three represent the crossover to insulating behavior. The large changes in the temperature dependence of the resistivity and sensitivity between samples A, B, and C produced by small changes in the oxygen flow rate from 0.13 to 0.17 sccm illustrate the sensitive dependence of the thermometer properties on the oxygen concentration. The relative effect of changes in the metal sputtering rate and the oxygen flow rate is illustrated by sample D, deposited at both a lower oxygen flow and a lower metal-deposition rate. An increase in the oxygen flow rate thus contributes to the crossover from metallic to insulating behavior in a manner similar to an increase in the SiO_2 sputtering rate.

These as-deposited films—capped by a thin insulating layer of SiO_2 to protect against humidity and further oxidation—are remarkably stable. To within the resolution of our measurements, no shifts in calibration were seen in samples remeasured 5 years later. With the exception of the highest resistivity samples (such as sample A in Fig. 2), no shifts in calibration were observed after annealing for 1 h at 350°C, nor after an additional 10 min at 380°C. For the highest-resistivity samples, a small decrease in resistivity is sometimes seen at low temperatures after a first anneal but no further changes are seen with additional anneals.

B. TEM

The plan-view TEM micrographs in Fig. 3 show cermet films grown at constant Ni-Cr and SiO_2 sputtering rates but with differing oxygen flow rates. The micrographs indicate that the change to more insulating properties arises from a decrease in the average metal-island size with

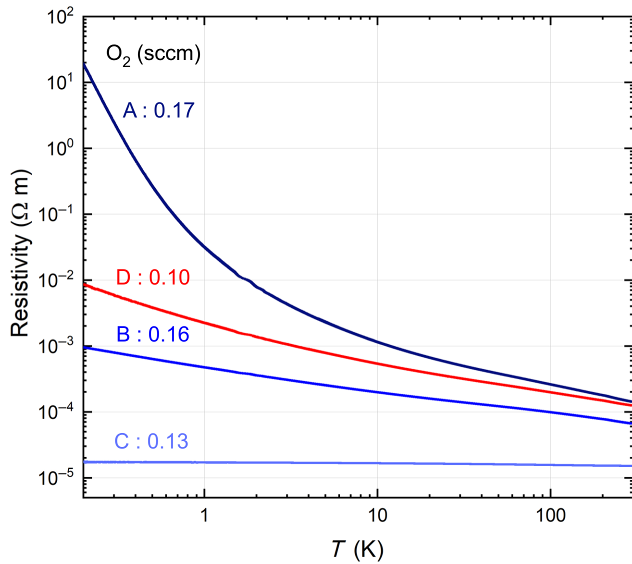

FIG. 2. Measured resistivities $\rho(T)$ for different oxygen flow levels during cosputtering. Increasing the oxygen flow rate induces a transition from metallic to insulating behavior. Films A, B, and C were deposited at a Ni-Cr rate of 2.81 nm/min and an SiO_2 rate of 0.78 nm/min, with oxygen flow rates of 0.17, 0.16, and 0.13 sccm, respectively. Film D was deposited at a Ni-Cr rate of 1.99 nm/min and an SiO_2 rate of 0.58 nm/min, with an oxygen flow rate of 0.10 sccm. In all cases, the argon-working-gas flow rate was 25 sccm. The dimensionless sensitivity of film D is nearly ideal for a wide-range sensor, increasing from 0.5 at 100 K to 1.0 at 0.2 K.

increasing oxygen concentration. Figure 4 shows TEM micrographs as a function of an increasing metal:insulator sputtering-rate ratio at constant oxygen concentration. The metal-island size at any given oxygen flow rate is seen to increase with an increasing metal:insulator sputtering-rate ratio. Samples grown without O_2 show the same trend—an increasing island size with greater metal content—but the island sizes tend to be larger when sputtered without oxygen, with sizes ranging from 4.0 nm for the 62.5% sample in Fig. 1 to 5.0 nm for the 68% sample.

C. Magnetic field dependence

In Fig. 5, the thermometer magnetoresistance is shown for magnetic fields up to 12 T and temperatures from 75 mK to 250 K. At low fields, the magnetoresistance is negative except for the lowest temperatures, $T < 1.1$ K, and the highest temperatures, $T \gtrsim 230$ K. The size of the negative-magnetoresistance term increases with decreasing temperature down to 40 K [see Fig. 5(c)] and then becomes smaller again at still lower temperatures [see Figs. 5(a) and 5(b)]. Near room temperature, the magnetoresistance is positive and linear with the field. The magnetoresistance at high magnetic fields increases linearly with the field at all temperatures, as seen in Fig. 6. For the studied samples, the zero-field dimensionless sensitivity varies between 0.28 and 0.38 over the temperature range. The maximum effect of the magnetic field on the apparent temperature at any temperature is only 2%.

IV. DISCUSSION

A. Temperature dependence

One useful physical model [29,30] for the temperature-dependent resistivity $\rho(T)$ of materials near the metal-insulator transition involves a crossover from variable-range hopping at the lowest temperatures to a nearly constant "disordered-film" resistance at high temperature. We represent this here by a phenomenological extended variable-range-hopping model incorporating a crossover from stretched exponential to augmented power-law dependence [29] for films close to the metal-insulator transition:

$$\rho(T) = \rho_0 \left[1 + \left(\frac{T_0}{T}\right)^{\nu}\right] e^{(T_0/T)^{\nu}}, \tag{1}$$

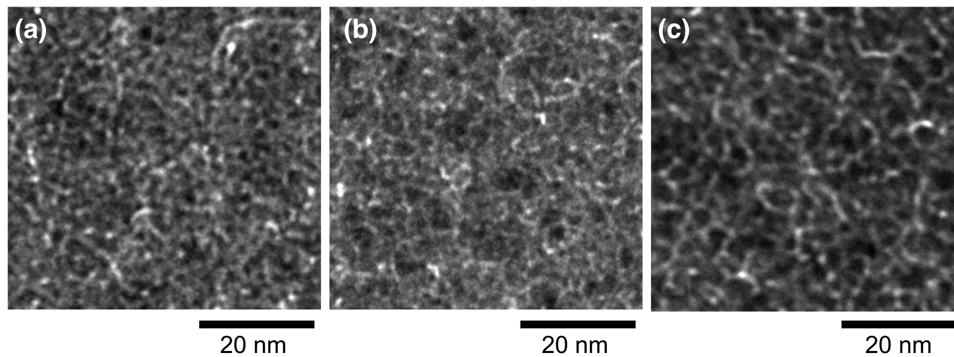

FIG. 3. Plan-view TEM micrographs of cermet films grown with varying O_2 flow conditions producing (a) higher than optimal, (b) optimal, and (c) lower than optimal ρ versus T characteristics. Larger metal-particle sizes correlate with lower sensitivity. All films are cosputtered in an Ar-O_2 mixture at a working pressure of 3 mTorr, with an argon flow of 25 sccm.

TABLE I. The film-growth parameters for Figs. 3 and 4.

Figure	Ni-Cr rate (nm/min)	SiO_2 rate (nm/min)	R_{RT} (kΩ)	O_2 flow (sccm)	Diameter (nm)
3(a)	2.10	0.58	30–35	0.15	3.1
3(b)	2.10	0.58	1.2–1.3	0.12	4.4
3(c)	2.10	0.58	0.43–0.48	0.10	5.7
4(a)	2.60	0.80	2.0–2.8	0.19	2.8
4(b)	2.74	0.80	1.5–2.0	0.19	3.2
4(c)	2.95	0.80	0.75–0.85	0.19	3.6

where $k_B T_0$ represents a characteristic energy for variable-range hopping between adjacent metal islands in an insulating medium, ν is a measure of the power-law sensitivity, the value of which depends (in part) on the distribution of the effective distances, and ρ_0 is a scaling parameter equal to the residual resistivity in the $T \to \infty$ high-temperature limit. ρ_0, T_0, and ν all depend on the metal-island percentage x.

We find that the $\rho(T)$ curves in Fig. 1 for (Ni-Cr, SiO_2) cermets cosputtered in a pure argon atmosphere are well described by Eq. (1) for Ni-Cr percentages near a metal-insulator transition at x_{MIT}; the dependence of ρ_0 on the metal concentration x can be modeled in terms of percolation theory [31]. Details and limitations of the modeling are discussed in the Appendix.

Experimentally, the residual resistivity ρ_0, the power-law coefficient ν, and the hopping temperature T_0 all decrease with an increasing metal percentage. As a result, materials described by this model exhibit a trade-off: an increasing sensitivity ν leads to a higher residual resistivity ρ_0.

There is a notable resemblance between the temperature dependence shown in Fig. 1 and that seen for 100-nm-thick $Ni_x(SiO_2)_{1-x}$ cermets [21] cosputtered in argon for atomic percentages ranging from $x = 0.6$ to $x = 0.9$, having Ni metal-island sizes ranging from 5 to 10 nm for insulating films.

We observe a room-temperature resistivity of 200 μΩ m at 62.5% Ni-Cr, while the reported value for 66% Ni cermet with a comparable temperature dependence is 670 μΩ m [21]. Comparable sensitivities lead to similar room-temperature resistivities, albeit at measurably higher metal percentages for the Ni-based than Ni-Cr–based materials. A main difference, however, is in the low-temperature sensitivity, which abruptly decreases below 2 K for the Ni-based cermets. This decrease in sensitivity around 2 K has also been seen for Pt-based cermets [20]. A second difference is the larger effect of magnetoresistance at low temperature when using the Ni-based films as thermometers [21].

Our results shown here in Fig. 1—in particular, the crossover from metallic to strongly temperature-dependent insulating behavior and low-temperature magnetoresistance—also bear some resemblance to results observed between 1 K and 4 K for thin-metal-film thermometers formed from a film consisting of discontinuous metal islands of Ni-Cr sandwiched between two thick SiO_x layers [32]. The temperature dependence above 4 K has not been reported, however, as the films studied in Ref. [32] are unstable at room temperature, typically increasing in resistance by an order of magnitude after 30 days.

B. Dimensionless sensitivity

Unlike the films sputtered in a pure Ar atmosphere (Fig. 1), the oxygen-grown films (Fig. 2) retain a higher sensitivity even at room temperature, combined with an even lower room-temperature resistivity, making these films suitable for calorimetry at temperatures up to and including room temperature. For film D in Fig. 2, the dimensionless sensitivity increases from a minimum of 0.5 at 100 K to a

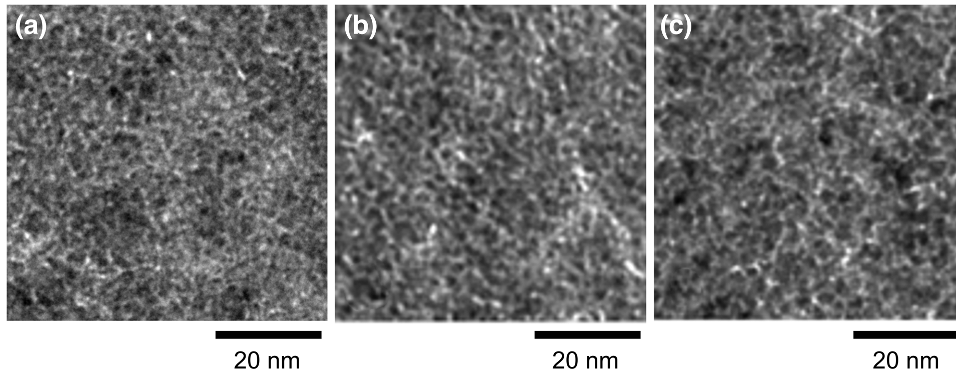

FIG. 4. Plan-view TEM micrographs of cermet films grown with varying metal sputtering rates producing (a) higher than optimal, (b) optimal, and (c) lower than optimal ρ versus T characteristics. Films with a higher metal rate (keeping the same O_2 flow rate and SiO_2 sputtering rate) lead to an increase in the average metal-island size. All films are cosputtered in an Ar-O_2 mixture at a working pressure of 3 mTorr, with an argon flow of 25 sccm.

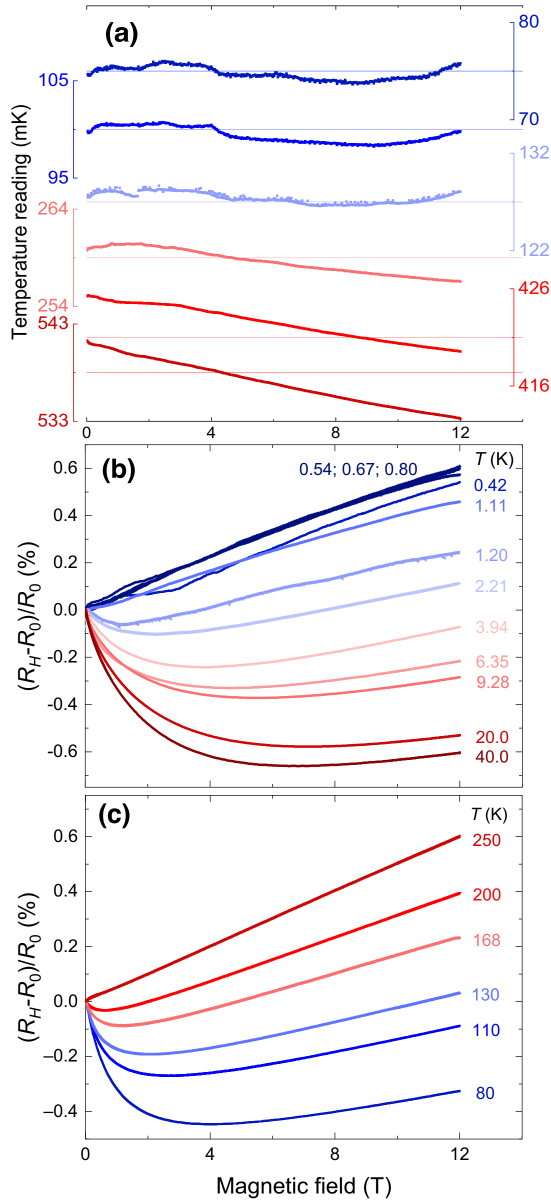

FIG. 5. The magnetoresistance as a function of the magnetic field up to 12 T, at various temperatures for (Ni-Cr, SiO_2) films cosputtered in O_2 and Ar at 3 mTorr pressure. The thermometer films have room-temperature resistivities around 7×10^{-5} Ω m and show a temperature dependence similar to film B in Fig. 2. (a) The measured temperature within 10-mK windows. Below 150 mK, the effect of the magnetic field sweep on the actual temperature affects the accuracy of the magnetoresistance. (b) magnetoresistance data below 40 K. (c) magnetoresistance above 40 K. The magnetoresistance at higher temperatures is composed of a negative low-field magnetoresistance and a linear positive high-field magnetoresistance.

maximum of 1.0 at 0.2 K, a sensitivity comparable to that seen in commercially available thin-film metal oxynitride ZrO_xN_y resistors [6]. In Fig. 7, curves with a comparable resistivity at 1 K, fabricated with Ar only and an Ar plus O_2 atmosphere, are compared. As seen in the figure,

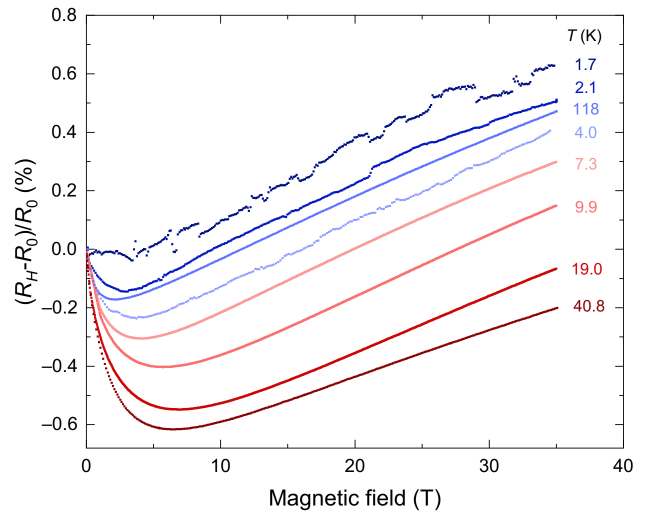

FIG. 6. The magnetoresistance as a function of the magnetic field up to 35 T at various temperatures, expressed as the relative resistance change. The curve at 1.7 K is affected by electronic noise, sporadically changing the temperature by a few millikelvin. The thermometer film has a room-temperature resistivity value of 9.17×10^{-5} Ω m and the temperature-dependence curve lies between films B and D in Fig. 2.

the room-temperature resistivity is significantly lower for the (Ar plus O_2)-grown samples. Within each preparation method, we also see that we can infer the low-temperature resistance of any particular (Ni-Cr, SiO_2) film from its room-temperature value. This implies that two identically prepared films with the same room-temperature resistivity should follow a common curve, as illustrated in the inset of Fig. 7. Sputtering in a reactive-oxygen atmosphere can be expected to change the resistive properties of the metal-alloy plus insulator cermets in at least two ways. First, sputtering in a reactive-oxygen atmosphere is expected to improve the stoichiometry of the sputtered SiO_2 [33,34] and may prevent the possible formation of metal silicides. Second, as the oxygen flow rate is increased, some Cr in $Ni_{0.8}Cr_{0.2}$ may react to form Cr_2O_3 due to the preferential oxidation of Cr. Put together, more insulator should be deposited when O_2 is present in the working gas. Consistent with this expectation, we find that we can use higher metal-deposition rates when using a dilute Ar-O_2 working-gas mixture instead of 100% Ar to obtain films with comparable room-temperature resistivity.

While the effect on cluster size with a changing metal:insulator ratio, shown in Figs. 3 and 4 is clear, the net effect for films with similar low-temperature behavior is rather subtle. Films grown in Ar behave similarly to those grown in Ar plus O_2. We find slightly larger island sizes for optimal films in the absence of oxygen but the effect is weak, less than approximately 1 nm. A more likely explanation for the effect of oxygen is that the barriers between clusters are improved, affecting the exponent ν

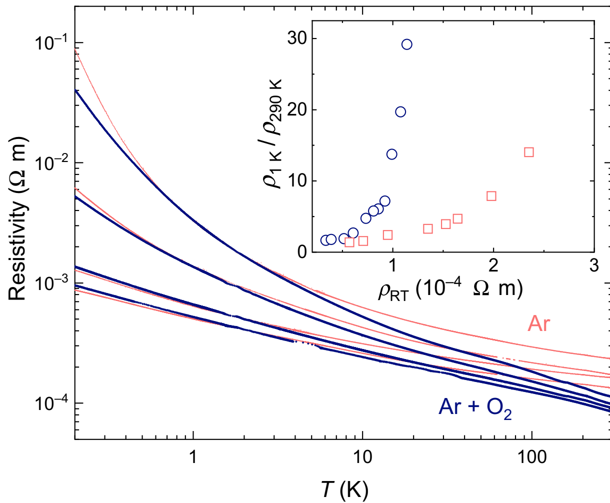

FIG. 7. A comparison of the temperature-dependent resistivities of (Ni-Cr, SiO_2) films fabricated in both Ar and Ar plus O_2 environments. Curves have been selected to match at about 1 K. Co sputtering in a reactive mixed Ar plus O_2 atmosphere yields films with significantly greater sensitivity between 10 K and room temperature. The inset describes the resistivity ratio as a function of the room-temperature resistivity for the two fabrication methods. Materials in the same fabrication family obey a common curve, allowing a quick comparison of materials.

of Eq. (1) and possibly increasing the metal:insulator ratio at the point of optimum low-temperature behavior, thereby lowering the high-temperature resistivity.

C. Magnetoresistance

For thermometry and calorimetry, lower magnetoresistance is always helpful, but it is the magnitude of the magnetic field induced effect on the temperature reading rather than the magnetoresistance itself that is the most important consideration. For the (Ni-Cr, SiO_2) sensors shown in Figs. 5 and 6, the magnetic field induced fractional change in the apparent temperature $\Delta T/T_0$ is less than 2% over the entire temperature and field ranges measured (75 mK to 300 K and 0–41 T). The low values of $\Delta T/T_0$ observed here are a significant improvement over that typically observed for ruthenium oxide sensors [5,16]—Ref. [5] reports a 28% change in $\Delta T/T_0$ at 0.62 K in a 32 T field—and cermets of comparable low-temperature sensitivity formed from elemental metals [19].

The positive magnetoresistance component at high fields has a linear field dependence and is nearly temperature independent, and is thus easily corrected for using methods that some of us have presented elsewhere [15]. The decrease in negative magnetoresistance with decreasing temperature is welcome but unusual. Over the same temperature range, the magnetic field induced change in resistance systematically increases as the temperature decreases for Cernox™ and related MO_xN_y thin film, Au-Ge thin film, and RuO_x thick-film resistors. An increase is also seen for the (Ni, SiO_2) cermet [21]. Our understanding of magnetoresistance in granular metals such as the cermets presented here is incomplete and continues to evolve [22,25,35]. That said, the most common explanation for negative magnetoresistance in elemental metals with long mean free paths is the destruction of coherent backscattering due to the application of the magnetic field. Coherent backscattering increases the resistivity of the material at zero field; destroying that coherence by magnetic field leads to a decrease in resistivity.

A main difference between pure-metal cermets and cermets based on alloys is the decreased mean free path of the alloy. A short enough mean free path minimizes any coherent backscattering and similar magnetoresistance effects. High-resistivity alloys, including Ni-Cr [36,37], are in the Mott-Ioffe-Regel limit [38,39], characterized by electronic mean free paths comparable to the interatomic distance. Comparing metals and various high-resistivity materials such as constantan, nichrome, and phosphor bronze, it is seen that the higher the ratio between room-temperature and low-temperature resistivity, the larger is the magnetoresistance at low temperature [40]. Thus, disorder-induced electron scattering by defects and introduced impurities are known to suppress magnetoresistance. Here, the isolated metal grains in combination with the use of a low-magnetoresistance metal alloy provides a means of producing a useful temperature dependence without introducing high magnetoresistance in a material with a mean free path that evidently remains in the Mott-Ioffe-Regel limit down to the lowest temperatures.

The role of combining different magnetic *d* elements for strong-disorder scattering at the Fermi level for high entropy alloys such as Ni-Cr is described in detail in Ref. [41]. In these materials, scattering can be understood in terms of disorder smearing of the Fermi surface, originating from potential site-to-site fluctuations [41]. The maximum disorder is obtained when there is a large band-center mismatch, such as that obtained by combining nearly filled *d*-band elements (ferromagnetic Fe, Co, Ni) with elements having half-filled *d* bands (antiferromagnetic Cr, Mn). This suggests that metal combinations that do not scatter strongly in both spin channels at the Fermi level will have a smaller but more temperature-dependent residual resistivity and, by implication, a larger magnetoresistance at the lowest temperatures.

The preferred choice of metal alloy for a particular cermet thermometry application will depend on additional considerations such as the magnetic susceptibility, the magnetic field dependence of the specific heat, and the suitability of the material for use in a sputtering system. In this regard, we have found promising indications that results similar to those presented here can be obtained by

replacing Ni-Cr with an arc-melted TiCr alloy (7% Ti by volume), which is sometimes used in calorimetric applications [42] as a less magnetic alternative to Ni-Cr for heater elements.

V. CONCLUSIONS

In conclusion, we have found that metal-ceramic composite thin films—in particular ($Ni_{0.8}Cr_{0.2}$, SiO_2)—fulfill all the requirements expected for thin-film-thermometer materials for measurement in high magnetic fields at low temperature. The use of a high-resistivity metal alloy greatly reduces the magnitude of the low-field magnetoresistance compared to that seen for oxygenated cermets formed from elemental metals [20,23]. The optimized thermometers display monotonic temperature dependence of the resistivity with a dimensionless sensitivity between 0.3 and 0.5, from 300 K to below 100 mK. They can be fabricated as stable square thin-film resistors with a predictable low-temperature sensitivity and their magnetoresistance is found to be less than 1% at all studied temperatures. Cosputtering the films in an atmosphere with a small amount of oxygen extends the useful temperature range of the resistive thin films by simultaneously increasing the sensitivity and decreasing the room-temperature resistivity (compared to sputtering in 100% Ar). The room-temperature resistivity and sensitivity can be further fine tuned by small changes in the metal-to-insulator sputtering rate ratio.

ACKNOWLEDGMENTS

Support from the Knut and Alice Wallenberg Foundation under Grant No. KAW 2018.0019 (N.K., A.R.) and the Swedish Research Council, Grant Number 2021-04360 (A.R.), is acknowledged. A portion of this work was performed at the National High Magnetic Field Laboratory, which is supported by the National Science Foundation (NSF) Cooperative Agreements No. DMR-1644779 and No. DMR-2128556 and the State of Florida. This work was also supported by the NSF Major Research Instrumentation (MRI) program, under Award No. 2018560. N.F., J.P.-F., and N.K. contributed equally to this work.

APPENDIX: EXTENDED VARIABLE-RANGE-HOPPING MODEL

In this appendix, we test the ability of the extended variable-range-hopping model [29] introduced to describe the temperature dependence of the resistivity (in the absence of an applied magnetic field). We also present corresponding graphs for the temperature-dependent logarithmic sensitivity S. We find that the model describes the temperature dependence of the cosputtered (Ni-Cr, SiO_2) films deposited in a pure-argon atmosphere at all temperatures—even at temperatures well above the characteristic hopping-energy temperature T_0—but fails to fully account for the temperature dependence of films cosputtered in a mixed argon plus oxygen atmosphere.

1. Variable-range-hopping model

We start with the expression given by Eq. (1) for the extended variable-range-hopping resistivity [29]. Expanding this expression in the high-temperature limit, using $\delta = (T_0/T)^{\nu} \ll 1$, gives

$$\rho(T)\bigg|_{T\to\infty} = \rho_0\,(1+\delta)\left(1+\delta+\frac{1}{2}\delta^2\cdots\right)\bigg|_{\delta\to 0} = \rho_0, \tag{A1}$$

indicating that the scaling parameter ρ_0 corresponds to the theoretically expected (constant) residual resistivity. The logarithmic sensitivity S is given by

$$S = -\frac{d\log R}{d\log T} = -\frac{T}{R}\frac{dR}{dT} = -\frac{T}{\rho(T)}\frac{d\rho(T)}{dT}, \tag{A2}$$

where the resistance R is related to the resistivity ρ as $R = (L/A)\rho$ for a thin film with length L, width w, thickness d, and cross-section area $A = wd$.

In calorimetry, the logarithmic sensitivity is important because the measurement resolution depends directly on the smallest resolvable temperature change, $\Delta T|_{\min}$. This is inversely proportional to S for a given minimum resolvable fractional change in resistance $(\Delta R/R)_{\min}$:

$$\Delta T\bigg|_{\min} = -\frac{1}{S}\left(\frac{\Delta R}{R}\right)_{\min} T \tag{A3}$$

Applying Eqs. (A1) to (A2) in the high-temperature limit, we find that

$$S\bigg|_{T>T_0} = 2\nu\left(\frac{T_0}{T}\right)^{\nu} \tag{A4}$$

In this $T > T_0$ approximation, a constant power-law sensitivity ν corresponds to an increasing numerical value for the logarithmic sensitivity as T decreases, with S expected to approach a reference value of 2ν as T approaches T_0.

2. Cermets sputtered in an inert argon atmosphere

Figure 8 shows fits of the empirical variable-range-hopping model [Eq. (1)] to data for various Ni-Cr concentrations. These represent a subset of the data presented in Fig. 1 for Ni-Cr percentages ranging from 63% to 66.5%. As seen in Fig. 8, the temperature-dependent resistivity $\rho(T)$ of these films can be fitted to the model of Eq. (1) over the entire temperature range from 0.2 K to 300 K. The

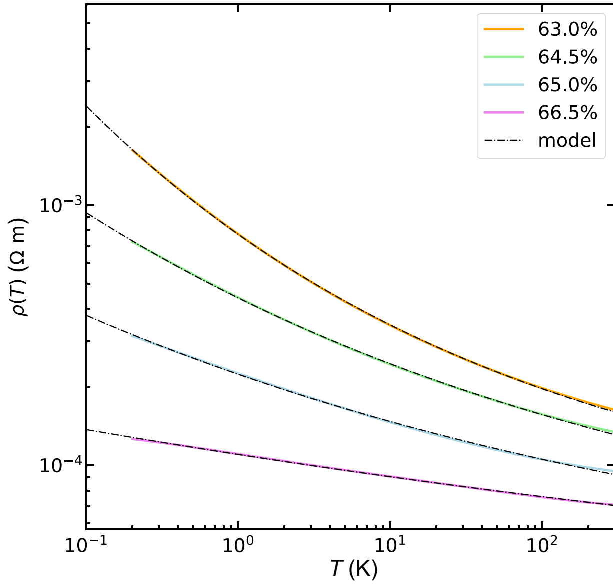

FIG. 8. The fit of the extended variable-range-hopping model to data for various Ni-Cr concentrations. The solid lines correspond to data and the dashed lines to the corresponding model fits to Eq. (1).

corresponding sensitivities for the data presented in Fig. 1 are shown in Fig. 9. Note how the slope dS/dT of the sensitivity changes from negative to positive as we cross the metal-insulator transition. The resulting fit parameters for films on the insulating side of the metal-insulator transition are listed in Table II.

As seen from Table II, the scaling temperature T_0 in this model does not appear independently of the power-law

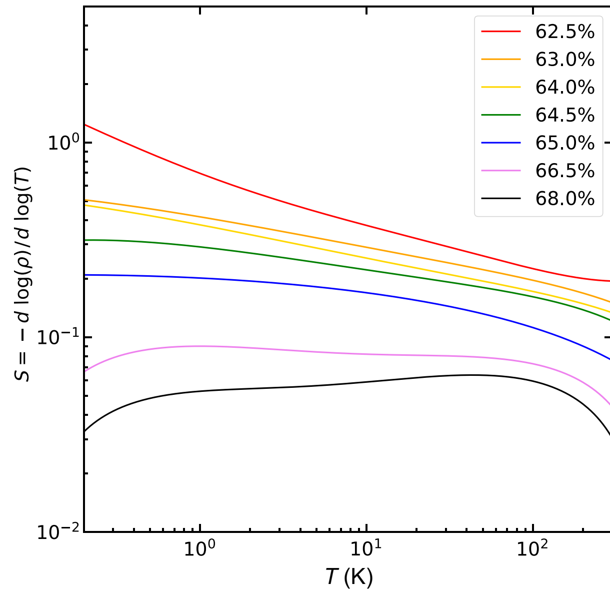

FIG. 9. The logarithmic (dimensionless) sensitivity S for the films shown in Fig. (1).

TABLE II. The dependence of the variable-range-hopping fitting parameters found from a nonlinear least-squares fit to Eq. (1) on the Ni-Cr metal percentage for (Ni-Cr, SiO_2) cermets cosputtered in pure argon.

Metal (%)	ρ_0 (μΩ m)	T_0 (K)	ν
63.0	57.0(2)	14.9(2)	0.183(2)
64.5	38.1(3)	22.3(4)	0.135(4)
65.0	30.6(4)	4.9(4)	0.116(1)
66.5	18.4(4)	3.0(7)	0.057(1)

sensitivity ν. Instead, it appears only in the combined expression ${T_0}^{\nu}$. As a result, we do not assign theoretical significance to the particular numerical values found here for T_0 and ν. For our purposes, it suffices to see that they combine to produce an overall decreasing logarithmic sensitivity S with an increasing metal percentage, as expected, and that the model given by Eqs. (1) and (A2) provides us with a useful means of estimating the temperature dependence of $\rho(T)$ and S from the measured room-temperature resistance.

The values for ρ_0 of Table II decrease as the metal percentage increases, as expected. However, the listed ρ_0 values are still an order of magnitude larger than the resistivity $\rho \approx 1.1$ μΩ m for nichrome ($Ni_{0.8}Cr_{0.2}$) [36]. From the TEM images, we see that the cermet structure consists of metal grains wrapped by insulator (rather than a uniform mixture of metal and insulator grains). Further, the 0.4-nm mean free path in Ni-Cr [36] is much smaller than the 2–5-nm Ni-Cr metal grain size, indicating that the enhanced resistivity is an intergrain effect [22]. We thus tentatively attribute the enhancement of ρ_0 to the proximity to the percolation threshold with narrow conduction paths through the material [31].

In the transition region of percolation near the percolation threshold [31,43,44], the conduction-path contribution to the resistivity is as follows:

$$\rho(x,T)\big|_{x\to x_c} = \alpha(T)\,(x/x_c - 1)^{-\beta} \quad \text{for } x > x_c\,, \tag{A5}$$

where x is the metal percentage, x_c is the percolation threshold—the metal percentage at which a narrow but continuous transport network is formed by the metallic grains—and $\alpha(T)$ represents the temperature dependence for a given x and x_c. β is a critical exponent that depends on dimensionality, with $\beta \to 2$ in the three-dimensional limit [31,44].

As the metal percentage decreases as x approaches x_c, the resistivity $\rho(x)$ at any fixed T increases and thus so does ρ_0 from our model. The critical value x_c depends on dimensionality and sample-preparation conditions, including deposition and annealing temperatures, as these can affect cluster sizes and distributions. Experimentally [31], values ranging from 0.54 to 0.62 have been observed for cosputtered Au and SiO_2. Here, if our materials are in this

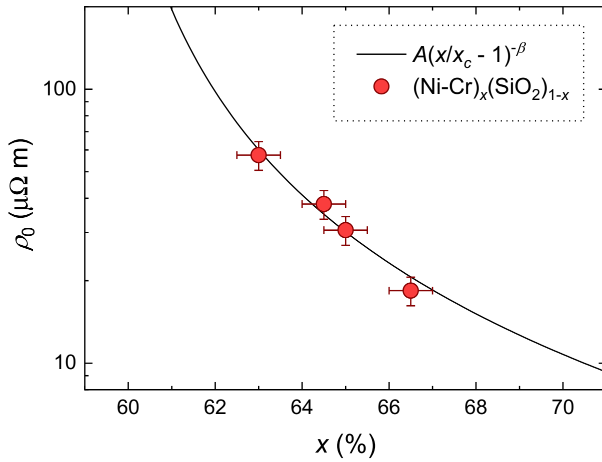

FIG. 10. The fit of the percolation model [Eq. (A5)] for the dependence of the residual resistivity ρ_0 to data presented in Table II. The calculated curve corresponds to a percolation threshold $x_c = 0.59 \pm 0.1$, with ρ_0 set equal to the bulk resistivity for Ni-Cr in the $x = 1$ continuous thin-film limit.

limit, then $x_c \leq 62.5\%$. A representative fit of Eq. (A5) to the data in Table II with $x_c = 0.59 \pm 0.1$, $\beta = 1.7 \pm 0.2$ and ρ_0 set equal to 1.15 μΩ m in the continuous Ni-Cr thick-film $x = 1$ limit is shown in Fig. 10.

In percolation theory [31], there is an intermediate weak-localization region between the classical percolation limit x_c and the classical metallic behavior for $x \geq x_{\mathrm{MIT}}$. As a result, the numerical value for the percolation threshold x_c calculated from the inferred high-temperature residual resistivity ρ_0 using Eq. (1) will be less than the numerical value for the metal-insulator transition x_{MIT} inferred from the measured low-temperature logarithmic sensitivity. Assigning x_{MIT} to the metal concentration at which dS/dT changes sign from positive to negative [29], we find $x_{\mathrm{MIT}} \approx 0.665$. Thus, with the exception of the $x = 0.68$ film, the (Ni-Cr, SiO_2) cermets presented here are in that intermediate regime, $x_c < x < x_{\mathrm{MIT}}$.

3. Cermets sputtered in a mixed argon plus oxygen atmosphere

The effect of cosputtering in a reactive-oxygen plus argon atmosphere on the temperature dependence of $\rho(T)$ is discussed in detail in the main text. Here, we add a graph of the dependence of the logarithmic sensitivity S for the insulating-side films shown in Fig. 2. As shown in Fig. 11, the sensitivity increases as the oxygen concentration increases. Attractively, film B exhibits a nearly constant sensitivity of $S \approx 0.4$ between 0.1 K and 100 K. The increase in sensitivity with increasing temperature above 100 K for the insulating-side films indicates that sputtering in a reactive-oxygen atmosphere introduces new physics near room temperature that is not included in Eq. (1).

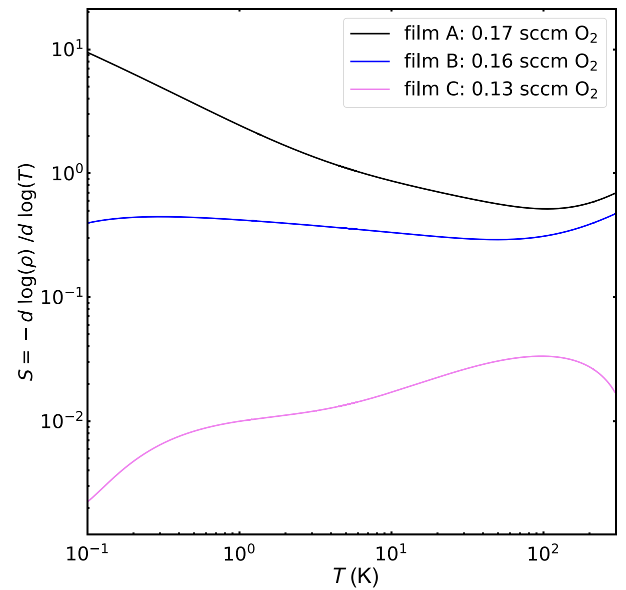

FIG. 11. The logarithmic (dimensionless) sensitivity S for a series of films sputtered in a mixed argon plus oxygen atmosphere at differing oxygen flow rates. These films correspond to the $\rho(T)$ graphs for films A, B, and C shown in Fig. 2. The slope dS/dT changes from negative to positive as the films change from metallic to insulating with increasing oxygen flow rate. The increase in sensitivity at high temperature that occurs in films A and B is not accounted for by the extended variable-range-hopping model in Fig. 8.

[1] S. Tagliati, V. M. Krasnov, and A. Rydh, Differential membrane-based nanocalorimeter for high-resolution measurements of low-temperature specific heat, Rev. Sci. Instrum. **83**, 055107 (2012).

[2] P. G. LaBarre, A. Rydh, J. Palmer-Fortune, J. A. Frothingham, S. T. Hannahs, A. P. Ramirez, and N. A. Fortune, Magnetoquantum oscillations in the specific heat of a topological Kondo insulator, J. Phys.: Condens. Matter **34**, 36LT01 (2022).

[3] N. Koppetzki, Thick film resistors in low-temperature resistance thermometry in high magnetic fields, Cryogenics **23**, 559 (1983).

[4] Q. Li, C. H. Watson, R. G. Goodrich, D. G. Haase, and H. Lukefahr, Thick film chip resistors for use as low temperature thermometers, Cryogenics **26**, 467 (1986).

[5] R. Goodrich, D. Hall, E. Palm, and T. Murphy, Magnetoresistance below 1 K and temperature cycling of ruthenium oxide–bismuth ruthenate cryogenic thermometers, Cryogenics **38**, 221 (1998).

[6] S. S. Courts, A standardized Cernox cryogenic temperature sensor for aerospace applications, Cryogenics **64**, 248 (2014).

[7] Z. Lin, G. Zhan, M. You, B. Yang, X. Chen, X. Wang, W. Zhang, and J. Liu, NTC thin film temperature sensors for cryogenics region with high sensitivity and thermal stability, Appl. Phys. Lett. **113**, 133504 (2018).

[8] P. Swinehart, S. S. Courts, and D. S. Holmes, Metal oxynitride resistance films and methods of making the same, U.S. Patent No. 5367285 (1994).

[9] B. W. Dodson, W. L. McMillan, J. M. Mochel, and R. C. Dynes, Metal-insulator transition in disordered germanium-gold alloys, Phys. Rev. Lett. **46**, 46 (1981).

[10] D. Zhu and F. Lin, Fabrication of Ge-Au film thermometers using interfacial atomic diffusion, Rev. Sci. Instrum. **64**, 2624 (1993).

[11] O. Béthoux, R. Brusetti, J. C. Lasjaunias, and S. Sahling, Au-Ge film thermometers for temperature range 30 mK–300 K, Cryogenics **35**, 447 (1995).

[12] N. A. Fortune, M. J. Graf, and K. Murata, Physical dependence of the sensitivity and room-temperature stability of Au_xGe_{1-x} thin film resistive thermometers on annealing conditions, Rev. Sci. Instrum. **69**, 133 (1998).

[13] J. R. A. Dann, P. C. Verpoort, J. Ferreira de Oliveira, S. E. Rowley, A. Datta, S. Kar-Narayan, C. J. B. Ford, G. J. Conduit, and V. Narayan, Au-Ge alloys for wide-range low-temperature on-chip thermometry, Phys. Rev. Appl. **12**, 034024 (2019).

[14] G. S. Boebinger, *National High Magnetic Field Laboratory 2021 Annual Report*, Tech. Rep. (National High Magnetic Field Laboratory, 2021), https://nationalmaglab.org/media/r0hd4tmh/areport˙2021.pdf.

[15] N. Fortune, G. Gossett, L. Peabody, K. Lehe, S. Uji, and H. Aoki, High magnetic field corrections to resistance thermometers for low temperature calorimetry, Rev. Sci. Instrum. **71**, 3825 (2000).

[16] G. G. Ihas, L. Frederick, and J. P. McFarland, Low temperature thermometry in high magnetic fields, J. Low. Temp. Phys. **113**, 963 (1998).

[17] J. Nelson and A. M. Goldman, Thin film cryogenic thermometers defined with optical lithography for thermomagnetic measurements on films, Rev. Sci. Instrum. **86**, 053902 (2015).

[18] R. Rosenbaum, B. Brandt, S. Hannahs, T. Murphy, E. Palm, and B. J. Pullum, Anomalous magnetoresistance behavior of an insulating zirconium oxynitride Cernox thermometer, Phys. B **294**, 489 (2001).

[19] B. Abeles, in *Applied Solid State Science*, edited by R. Wolfe (Elsevier, Amsterdam, 1976), Vol. 6, p. 1.

[20] N. A. Gershenfeld, J. E. VanCleve, W. W. Webb, H. E. Fischer, N. A. Fortune, J. S. Brooks, and M. J. Graf, Percolating cermet thin-film thermistors between 50 mK–300 K and 0–20 T, J. Appl. Phys. **64**, 4760 (1988).

[21] K. M. Unruh, B. M. Patterson, J. R. Beamish, N. Mulders, and S. I. Shah, Granular (Ni, SiO_2) thin films as low temperature thermometers, J. Appl. Phys. **68**, 3015 (1990).

[22] I. S. Beloborodov, A. V. Lopatin, V. M. Vinokur, and K. B. Efetov, Granular electronic systems, Rev. Mod. Phys. **79**, 469 (2007).

[23] N. A. Gershenfeld, J. V. Cleve, M. J. Graf, N. A. Fortune, and J. S. Brooks, Versatile low temperature and high magnetic field thermometers: The low temperature magneto resistance of thin film cermets, Jpn. J. Appl. Phys. **26**, 1741 (1987).

[24] B. Patterson, M. Allitt, K. Unruh, J. Beamish, and P. Sheng, Transport properties of metallic granular metal thin films, Nanostructured Mater. **1**, 245 (1992).

[25] P. Sheng, Eelectronic transport in granular metal films, Philos. Mag. B **65**, 357 (1992).

[26] N. A. Fortune, J. S. Brooks, M. J. Graf, G. Montambaux, L. Y. Chiang, J. A. A. J. Perenboom, and D. Althof, Specific-heat study of the anomalous quantum limit of $(TMTSF)_2(ClO_4)$, Phys. Rev. Lett. **64**, 2054 (1990).

[27] J. E. Palmer, Ph.D. thesis, Department of Electrical Engineering and Computer Science, Massachusetts Institute of Technology, 1989.

[28] A. Romano, J. Vanhellemont, H. Bender, and J. Morante, A fast preparation technique for high-quality plan view and cross-section TEM specimens of semiconducting materials, Ultramicroscopy **31**, 183 (1989).

[29] A. Möbius, The metal-insulator transition in disordered solids: A critical review of analyses of experimental data, Crit. Rev. Solid State Mater. Sci. **44**, 1 (2019).

[30] A. Mobius, C. Frenzel, R. Thielsch, R. Rosenbaum, C. J. Adkins, M. Schreiber, H.-D. Bauer, R. Grotzschel, V. Hoffmann, T. Krieg, N. Matz, H. Vinzelberg, and M. Witcomb, Metal-insulator transition in amorphous $Si_{(1-x)}Ni_{(x)}$: Evidence for Mott's minimum metallic conductivity, Phys. Rev. B **60**, 14209 (1999).

[31] S. P. McAlister, A. D. Inglis, and P. M. Kayll, Conduction in cosputtered Au-SiO_2 films, Phys. Rev. B **31**, 5113 (1985).

[32] E. L. Griffin and J. M. Mochel, Low temperature, thin film NiCr thermometers, Rev. Sci. Instrum. **45**, 1265 (1974).

[33] R. E. Jones, H. F. Winters, and L. I. Maissel, Effect of oxygen on the rf-sputtering rate of SiO_2, J. Vac. Sci. Technol. **5**, 84 (1968).

[34] S.-H. Jeong, J.-K. Kim, B.-S. Kim, S.-H. Shim, and B.-T. Lee, Characterization of SiO_2 and TiO_2 films prepared using rf magnetron sputtering and their application to anti-reflection coating, Vacuum **76**, 507 (2004).

[35] B. Aronzon, S. Kapelnitsky, and A. Lagutin, in *Thin Films and Nanostructures* (Elsevier, Amsterdam, 2007), Vol. 34, p. 581.

[36] J. H. Mooij, Electrical conduction in concentrated disordered transition metal alloys, Phys. Status Solidi (A) **17**, 521 (1973).

[37] G. D. Samolyuk, S. Mu, A. F. May, B. C. Sales, S. Wimmer, S. Mankovsky, H. Ebert, and G. M. Stocks, Temperature dependent electronic transport in concentrated solid solutions of the 3*d*-transition metals Ni, Fe, Co and Cr from first principles, Phys. Rev. B **98**, 165141 (2018).

[38] A. F. Ioffe and A. R. Regel, Non-crystalline, amorphous and liquid electronic semiconductors, Prog. Semicond. **4**, 237 (1960).

[39] N. F. Mott, Conduction in non-crystalline systems IX. The minimum metallic conductivity, Philos. Mag. **26**, 1015 (1972).

[40] M. Abrecht, A. Adare, and J. W. Ekin, Magnetization and magnetoresistance of common alloy wires used in cryogenic instrumentation, Rev. Sci. Instrum. **78**, 046104 (2007).

[41] S. Mu, G. D. Samolyuk, S. Wimmer, M. C. Troparevsky, S. N. Khan, S. Mankovsky, H. Ebert, and G.

M. Stocks, Uncovering electron scattering mechanisms in NiFeCoCrMn derived concentrated solid solution and high entropy alloys, npj Comput. Mater. **5**, 1 (2019).

[42] R. E. Schwall, R. E. Howard, and G. R. Stewart, Automated small sample calorimeter, Review of Scientific Instruments **46**, 1054 (1975).

[43] B. Dorfman, Critical parameters of percolation in metal-dielectric diamond-like composites of atomic scale, Thin Solid Films **330**, 76 (1998).

[44] G. Lewis, Z. Moktadir, M. Kraft, and L. Jiang, Resistivity percolation of co-sputtered amorphous Si/Ti films, Mater. Lett. **63**, 215 (2009).